An effective improvement for enhancing the strength and feasibility of FRP spike anchors

Wei Sun[a,b], Shukui Liu[c], Chunyang Zhang[a]

[a] Key Laboratory of Ministry of Education for Mechanics on Western Disaster and Environment, School of Civil Engineering and Mechanics, Lanzhou University, Lanzhou 730000, China

[b] School of Engineering, University of Southampton, Southampton, SO17 1BJ, UK

[c] School of Mechanics and Civil Engineering, China University of Mining and Technology, 221116, China

Abstract

Spike anchors are promising remedies to prevent the debonding failure of FRP sheets. The performance of anchored FRP sheets largely depends on critical parameters such as the extending bond length of FRP sheet over the embedded spike and bend radius, greatly limiting their efficiency and feasibility in field. Moreover, their long-term performance dealing with possible bond loss is still unknown. Recently, an anchorage system consisting of a spike anchor and two patches has been developed. This anchorage system was expected to have several advantages over conventional spike anchors, which were rarely explored but are presented in this paper. A total of 21 experiments have been conducted to demonstrate their merits in terms of higher anchor strengths and minimizing the impacts of the extending bond length over the embedded spike, bend radius and FRP-concrete bond. Experimental results also suggest a great remedy to further improve the anchor efficiency by reducing the fanning angle. Thus, the proposed system could be considered as an efficient and feasible anchorage for FRP sheets.

Keywords: Spike anchor; Anchorage system; Bond length; Bend radius; FRP-concrete bond; Fanning angle

1. Introduction

Light, strong and non-corrosion FRP composites [1–4] offer a quick method for externally strengthening concrete structures. However, a premature FRP debonding from concrete substrate greatly compromises the high-strength merit of FRP material [5]. Various anchors have been therefore developed to make fuller use of externally bonded (EB) FRP sheets by preventing the premature debonding failure. Metal anchors consisting of bolts and plates are able to effectively delay EB FRP debonding from concrete substrate [6,7]. Nevertheless, the external application of metal anchors might need a specific anti-corrosion treatment. Notable stresses concentrated in the vicinity of metal-FRP connections could also compromise their applications in field. In order to address those issues, anchorages tend to be made by the same FRP material as that is used for EB FRP sheets, i.e. FRP anchors.

FRP strips with the fiber oriented perpendicular to the tensile direction were applied to delay the debonding process of EB FRP sheets [8]. However, this method might not be highly effective unless the strip was notably prestressed. A promising remedy could be wrapping EB FRP sheets with U-shape FRP strips [9–11]. Although U-wrapping anchors were able to prevent the premature debonding failure, they inherently required notably more FRP material to make the anchors and more surface preparation for installing the anchors on the sides of concrete elements. Meanwhile, FRP spike anchors have been gaining more and more attention because of their high-efficiency, easy-installation and small-size merits. As shown in Fig.1 (a), FRP spike anchors are installed by embedding one end into concrete elements and fanning out the other end bonded on the EB FRP sheet [12,13]. While the EB FRP sheet starts debonding from concrete substrate, the spike anchor is able to provide an alternative load-transferring mechanism for preventing the debonding failure. Current investigations suggest that key parameters, e.g. embedment depth (h_e), bend radius (R_b) and embedded angle (α_e) (see Fig. 1 (b)) determines both the capacity and failure mode of anchored EB FRP sheets [14]. In order to prevent an anchorage system being pulled off, the minimum embedment depth was recommended to be at least 100 mm or 4 inch [15]. A 13-mm-radius bend was suggested to prevent spike anchors being prematurely cut off [16]. Embedded angle can be used to determine the stress state [17]. Existing studies also demonstrate the impact of anchor strength and hole diameter (d_h) on the behavior of anchored EB FRP sheets [14,18]. An adequate strength ratio of FRP anchor to EB FRP sheet (S_{ratio}) is suggested to be no less than 2 by previous studies [5]. The hole diameters are determined by the diameter of anchor dowel (d_a). The diameter ratio of hole to anchor dowel is expected to be greater than 1.5 and no more than 2.2 [16]. Moreover, EB FRP sheets are recommended to be extended over the anchor dowel. As shown in Fig. 1 (b), the distance from anchor dowel to the corresponding end of EB FRP sheet (l_{end}) should be more than 225 mm to realize the nominal anchor strength [19]. This might suggest feasible issues in the usage of spike anchors to shear strengthen reinforced concrete elements with a limited depth. Another limitation of current spike anchors could be short of a ready method to control the bend radius (R_b) in field. The real radius might therefore vary from case to case, suggesting a possibly overestimated anchor strength obtained from a nominal bend radius. In order to make a fuller usage of EB FRP material, the fanning angle α_f (see Fig. 1 (c)) is also expected to be properly adjusted so that the entire width of EB sheets can be fully covered by the fanned out anchor [16]. Recently, a FRP anchorage system consisting of a spike anchor and two FRP patches have been developed to improve the reliability of conventional FRP spike anchors [5,16,20,21]. It was also found that this anchorage system could make fuller use of EB FRP sheet than conventional spike anchors did [21].

In this study, three-point bending tests have been conducted to demonstrate the merits of the anchorage system. That is increasing the apparent anchor strength and minimizing the impacts of l_{end} and R_b. The performance of the anchorage system for partially unbonded FRP sheets has also been studied. Those partially unbonded tests were conducted to simulate possible bond loss between two anchorage systems under the natural impact of UV light and heat [22,23]. Compared with fully bonded tests, capacity loss was observed from those partially unbonded tests. This observation provides with valuable data for evaluating the durability of the anchored EB FRP system. Moreover, the study has explored a possible method (i.e. adjusting the fanning angle) to further improve the anchorage system.

2. Current design recommendations on spike anchors

JSCE [24] (Eq. (1)) and ACI [25] (Eq. (2)) have published empirical equations in the usage of the nominal FRP strength f_{fu} and bend ratio r_b to determine the ultimate bend strength f_{fb} for internal reinforcements. Those equations have been validated by experiments [25–27], and are shown as follows:

$$f_{fb} = (0.07r_b + 0.45)f_{fu} \quad (1)$$

$$f_{fb} = (0.05r_b + 0.3)f_{fu} \quad (2)$$

in which

$$r_b = R_b/d_a \quad (3)$$

A recent study has modified those empirical equations by including the impact of embedded depth (h_e) and angle (α_e in degrees) [14]. The modified equation is shown as follows:

$$f_{fb} = (0.3h_e/150 + 0.5r_b\alpha_e/90^0)f_{fu} \quad (4)$$

Another recently developed equations have included the strength ratio of FRP anchor to EB FRP (S_{ratio}) [21]. The equation can be expressed as:

$$f_{fb} = f_{fu}\left[(0.06r_b + 0.21) + 0.22S_{ratio}^{-1.15} + 0.23(\alpha_e/90^0 - 1)\right] \quad (5)$$

It should be noted that those equations provide with valuable tools to determine the strength of conventional spike anchors, which could be greatly improved by using the proposed anchorage system consisting of FRP anchors and patches.

3. Experiments

As shown in Fig. 2, three-point flexural tests have been conducted to determine the strength of anchored EB FRP sheets installed on the tensile surface of test specimens (see Fig. 3 (a)-(b)). Specimens were concrete blocks with a constant dimension of 152×152×610 mm^3 as shown in Fig. 3 (b)-(c). Two separated U-shape FRP strip were applied on the sides of specimens to prevent concrete shear failure. A 25 mm cut was made at the midspan to control the cracking path. The test setup and specimens were developed exclusively for isolating anchor behavior [16]. More details can be found in literature [16].

Tyfo sch-11 up [28] was used to fabricate EB FRP sheets with a dimension of 127×482 mm^2 and FRP anchorage systems. The FRP strength ratio of anchor to sheet at any section was a constant value of 2.0. Direct tensile tests in accordance with ASTM D3039 were conducted on five 15×240 mm^2 FRP coupons with 15×40mm^2 FRP end-tabs. The average values of modulus E_f and ultimate strain ε_f were 95.7 GPa and 0.011, respectively. The manufacturer-specified values (e.g. laminate thickness=0.51 mm, tensile modulus= 95.8 GPa and ultimate strain=0.01) stemmed from more experimental results were very close to measured values, and will be applied in the following studies. According to Chinese code GB 50010, the average concrete strength obtained from five cubic specimens with a dimension of 150×150×150 mm^3 was 36 MPa (or 28 MPa for cylinder strength).

In the group consisting of specimen No. 1-9 (see Table 1), all tests have identical FRP systems expect for the patch arrangement. Conventional spikes with no patches (NP) have been applied for the first three specimens, i.e. No. 1-3 in Table 1. Then, transverse patches (TP) have been used for another three specimens (No. 4-6) to improve the load transferring mechanism within a short l_{end} of 38 mm. For specimen No. 7-9, both transverse and longitudinal patches (TLP) have been applied to achieve further improvements. Those patches had a constant dimension of 127×127 mm^2. All spike anchors were inserted into pre-drilled holes with a bend radius of 13 mm (R13), then fanned 49° (F49) to fully cover the EB FRP sheet. The group consisting of specimen No. 10-15 was applied to demonstrate the impact of bend radius and bond loss on the anchorage system with both transverse and longitudinal patches. All specimens had a fanning angle of 49° in this group in which specimen No. 10-12 have a 0 mm bend radius. A plastic film was preseted for specimen No. 13-15 to prevent any FRP-concrete bond within the 127×228 mm^2 unbonded area while two-patch regions with an area of 127×127 mm^2 were well bonded on concrete substrate as shown in Fig. 3 (a). Specimen No. 16-21 were tested to demonstrate the impact of reducing fanning angle (from 49° to 37°) on various radius scenarios (R0 and R13) and bond conditions. The bend radius of specimen No. 16-18 and specimen No. 19-21 are 0 mm (R0) and 13 mm (R13), respectively. Moreover, the bond condition of specimen No. 16-18 and specimen No. 19-21 are well bonded and partially unbonded, respectively. As listed in Table 1, the nomenclature used for identifying experiments are bond condition (i.e. B and U stands for bonded and partially unbonded)-patch arrangement (i.e. NP for no patch, TP for transverse patch or TLP for transverse + longitudinal patch)-bend radius (i.e. R13 or R0)-fanning angle (i.e. F49 or F37)-experiment ID (a, b, and c).

Applied loads were recorded by the load cell of the testing machine CSS-WAW1000DL. Deflections were the relative displacements between the midspan and two supports. A camera system (DO3THINK U3S1250M-H) was used to measure those displacements. Fig. 4 shows that the predicted ultimate load P_u obtained from the nominal ultimate force of the EB FRP sheet at midspan F_{uf} by using the following expressions with w_s= specimen width, mm, c=depth of neutral axis, mm, A_f= section area of the FRP sheet, mm^2, ε_c= the ultimate compressive strain of concrete, $f_c^{'}$ =specified compressive stress of concrete, MPa, ($f_{cu} = f_c^{'}/0.78$):

$$F_{uf} - F_{uc} = 0 \tag{6}$$

$$P_u/2 \times L_{ps} - F_{uf} \times (h_f - \mathrm{c}) - M_{uc} = 0 \tag{7}$$

$$F_{uf} = \begin{cases} A_f \varepsilon_f E_f \;\; if \; A_f \varepsilon_f E_f \leq A_a f_{fb} \\ A_a f_{fb} \;\; if \; A_f \varepsilon_f E_f > A_a f_{fb} \end{cases} \tag{8}$$

$$F_{uc} = w_s c f_c^{'} \left[\varepsilon_c/\varepsilon_0 - (\varepsilon_c/\varepsilon_0)^2/3 \right] \tag{9}$$

$$M_{uc} = w_s c^2 f_c^{'} \left[2\varepsilon_c/3\varepsilon_0 - (\varepsilon_c/\varepsilon_0)^2/4 \right] \tag{10}$$

$$\varepsilon_0 = 1.8 f_c^{'}/E_c \tag{11}$$

$$\varepsilon_c = \varepsilon_f c/(h_f - c) \tag{12}$$

$$A_a = d_a^2 \pi/4 \tag{13}$$

Force and moment equilibrium were applied to obtain the two unknowns (P_u and c). The span from the applied load to the support (L_{ps}) was 267 mm. The relative FRP height (i.e. h_f) was 152 mm. The compression force F_{uc} and the corresponding moment M_{uc} were obtained from integrating the concrete stress f_c at the compressive region. The concrete stress is given as follows [29]:

$$f_c = f_c^{'}(2\varepsilon_c/\varepsilon_0 - (\varepsilon_c/\varepsilon_0)^2) \tag{14}$$

4. Results and discussion

A total of 21 experiments have been conducted to demonstrate the merits of the anchorage system in terms of minimizing the impact of l_{end}, r_b and bond condition. Those improvements are presented and discussed in this section. The section also explores a feasible remedy to further improve the anchorage system.

4.1 Conventional spike anchor

The results of three experiments (No. 1-3) using conventional spike anchors are presented in this section. They served as control tests to demonstrate the performance of selected equations and the improvements achieved by the anchorage system. Fig. 5 (a) shows the load-deflection curves of the three experiments. All curves clearly suggest two distinctive stages. Firstly, increasing the applied load results in slightly increased deflections, producing stiff linear responses. Notably deflections were gradually developed by further increasing the applied load up to the ultimate, suggesting spike anchors successfully transferring the tensile force from EB FRP sheets into concrete specimen. All specimens eventually failed because of the delamination between the anchor and the sheet as shown in Fig. 5 (b). This suggests that a 38 mm bond length extending over the conventional spike anchor or a spike anchor having a l_{end}=38 mm is inadequate to fully develop the strength of the anchor or sheet. Nevertheless, the range of the ultimate loads has been reasonably captured by implementing anchor strengths (Eq. (1)-(5)) into force and moment equilibrium equations (Eq. (6)-(7)). As listed in Table 2, all equations except for Eq. (1) tend to underestimate the ultimate load. The best agreements are made by Eq. (5) which achieves around 88% (365MPa/413MPa) of the measured loads. It also illustrates that those ultimate loads are much lower than the predicted load (69 kN) to fracture EB FRP sheet (see Fig.5 (a)), suggesting the potential of improving the conventional FRP spike anchor. In the following sections, experimental-based comparisons between spike anchors and the proposed anchorage system are made to demonstrate the improvements. Those selected equations (Eq. (1)-(5)) are also applied as additional references to support the anchorage system.

4.2 Improvement of the anchorage system on $\boldsymbol{l_{end}}$

In this section, patches have been applied to improve the performance of the spike anchor having a short l_{end} (i.e. l_{end}=38 mm). Transverse-patches were first applied for three experiments (No. 4-6) to mitigate the anchor delamination. Then, an upgraded system, i.e. the two-patch system, has been used for another three experiments (No. 7-9). All FRP details are identical in experiment No. 1-9 expect for patch arrangements (see Table 1).

As shown in Fig. 6 (a), all transverse-patch experiments (No. 4-6) develop two-stage loading curves similar to that of the comparable experiments using conventional spike anchors (No. 1-3). Two out of three specimens failed in ultimate loads which were unable to fracture the EB FRP sheets as shown in Fig. 6 (a). Moreover, all experiments failed in anchor-sheet delamination. This suggests that the transverse-patch arrangement cannot fully develop the tensile strength of FRP sheets. Nevertheless, transverse-patch experiments achieve notably larger loads than that of the comparable experiments (No. 1-3) as listed in Table 2, demonstrating their improvements. The slight torsion end (see Fig. 6 (b)) might suggest an uneven fiber distribution in the fanning region, resulting in an uneven force distribution and then producing the delamination between the anchor and the sheet.

In order to prevent the delamination failure, two patches consisting of both transverse and longitudinal patches have been applied in experiment No. 7-9. The introduction of longitudinal patches aim to minimize the impact of unevenly fanning out fibers. Moreover, longitudinal patches are able to increase the tensile stiffness in the anchor region, limiting the relative FRP-concrete slip [5,20]. The anchor region might therefore remain completely bonded on concrete substrate until the ultimate failure. The remaining bond would help to transfer the tensile force, increasing the apparent strength of the anchorage system. Transverse patches were then applied to minimize the impact of angled fibers due to fanning out, further smoothing the force-transferring mechanism and preventing the anchor-sheet delamination and anchor rupture. Therefore, the application of the two-patch system was expected to achieve 1) a higher apparent capacity by keeping the anchored region well bonded until the ultimate failure, and 2) delivering a better force-transferring mechanism to prevent anchor-sheet delamination and anchor rupture. As listed in Table 2 and Fig. 7 (a), all two-patch experiments developed notably ultimate loads that were able to fracture the FRP sheet. Their improvements were even much more notably by comparing their strengths with the corresponding strengths of conventional spikes and transverse-patch applications as shown in Fig. 7 (b). Possible variations of loading condition, installation quality and specimen material produced diverse failure modes. One experiment fractures the FRP sheet at 83 kN, and the rest ruptures the anchors at 82 kN and 91 kN, respectively. The typical failures of sheet fracture and anchor rupture are shown in Fig. 7 (c). Those observations suggest that the two-patch anchorage system is able to prevent the failure of anchor delamination, and to more efficiently transfer the tensile force even within a short l_{end} (i.e. l_{end}=38 mm). Compared with conventional spike anchors, the two-patch anchorage system effectively reduces l_{end} from 225 mm to 38 mm, and tends to fully develop the tensile strength of FRP sheets. This might suggest a more readily application for shear strengthening of the element with a limited depth. Those improvements favor the two-patch anchorage system to be a greater alternative for EB FRP sheets.

4.3 Impact of $\boldsymbol{R_b}$ and bond condition on the anchorage system

This section explores the impacts of bend radius and bond loss on the two-patch anchorage system with a short l_{end}=38 mm. The introduction of the proposed anchorage system was expected to achieve a higher reliability by minimizing the impact of those two parameters. Three experiments (No. 10-12) have been conducted to simulate the worst scenario in which the two-patch anchorage system deals with a sharp corner, i.e. R_b=0 mm. Another three experiments (No. 13-15) are conducted to demonstrate the performance of the anchored EB FRP sheet with no FRP-concrete bond (or bond loss) in the region between two adjacent patches. Then, anti-delamination measures could be more efficiently and effectively applied. All details are the same in experiments (No. 7-15) except for bend radius and bond condition.

Even dealing with a sharp corner (R_b=0 mm), the two-patch anchorage system developed adequate ultimate loads which were able to fracture FRP sheets as shown in Fig. 8 (a). Compared with those corresponding experiments having a smooth bend (R_b=13 mm), the sharp-corner experiments (No. 10-12) also achieved comparable ultimate loads (74 kN, 90 kN and 73 kN) as listed in Table 2 and Fig. 8 (b). This suggests a slight impact of bend radius on the strength of the two-patch anchorage system. The patches were applied to enlarge the bonded area from one point for embedding conventional FRP spikes to a rigid area. The enlarged anchorage area would remain well bonded until the ultimate failure, and it therefore was expected to provide additional load-transferring mechanism for compromising the bending impact. Although all sharp-corner experiments failed in the delamination (see Fig. 8 (c)), one delamination failure reached 90 kN which was much larger than that of anchor-rupture and sheet-fracture experiments (82kN in No. 7 and 83kN in No. 9), suggesting the merit of the anchorage system dealing with a sharp corner.

Fig. 9 (a) illustrates the load-deflection curves of those partially unbonded experiments. At the ultimate, the delamination might result in stress redistribution within the anchored region, producing several reloading processes. As listed in Table 2 and Fig. 9 (a)-(c), all experiments eventually failed in the delamination, developing ultimate loads no less than the prediction based on the sheet fracture. Nevertheless, those experiments fail in smaller ultimate loads than that of comparable tests with a well bond condition (No. 7-9 see Fig. 9 (b)). Those observations demonstrate possibly impacts of bond loss on the failure mode and the strength of the anchored EB FRP sheet.

In short, experimental observations demonstrate slight impacts of bend radius with a short l_{end}=38 mm and possible strength loss because of bond condition. In order to minimize the impact of those two critical factors, remedies can be made to prevent the delamination failure, and further improve the anchor efficiency.

4.4 Impact of fanning angle

Fanning angle was considered to have limited impact on the anchor strength as long as specimens failed in sheet fracture [5]. In this study, several experiments failed in either anchor delamination or anchor rupture suggesting a demand for improving the two-patch anchorage system. Reducing the fanning angle could improve the bond condition by enlarging the bond length between the anchor and the sheet, and increase the efficiency of the force transferring from the sheet to the anchor [30–33]. A reduced angle of 37° has been therefore applied to improve the anchorage system for three sharp-corner specimens (No. 16-18) and three partially unbonded specimens (No. 19-21).

By reducing the fanning angle, all three sharp-corner specimens (No. 16-18) developed much smoother load-deflection curves, suggesting limited delamination between the anchor and the sheet (Fig. 10 (a)). As listed in Table 1, a 37° angle achieved an around 20% larger anchored area than the one with 49° fanning angle, suggesting a stiffer anchored region. This stiffer region would help to limit the anchor-sheet slip, and prevent anchor-sheet debonding and anchor rupture. All specimen No. 16-18 failed because of sheet fracture (see Fig. 10 (b)), developing comparably ultimate loads to those standard two-patch tests (No. 7-9 see Fig. 10 (c)) with a smooth bend (R13) and a larger fanning angle (F49). As shown in Fig. 11 (a), all partially unbonded tests developed smooth load-deflection curves, suggesting loads transferring well from the sheet to the anchor with minimum impacts of anchor delamination. Two out of three partially unbonded specimens failed in sheet fracture, developing comparable ultimate loads to that of corresponding tests (No. 7-9 see Fig. 11 (b)) with a well bond condition. The rest one failed because concrete cover peeled off as shown in Fig. 11 (c). Without an adequate bond condition, the tensile force was primarily distributed by a small region of concrete around the anchor, resulting in stress concentration and concrete failure. This failure mode was not effectively prevented by reducing the fanning angle from 49° to 37°. In short, reducing the fanning angle was able to improve the load transferring from the sheet to the anchor, preventing the anchor delamination and anchor rupture. Nevertheless, the reduced angle might not be able to prevent the failure of concrete peel off.

5. Conclusions

Failure modes and ultimate loads of experiments have been applied to demonstrate the merits of the anchorage system. They are listed as follows.

1. Compared with conventional spike anchors, the anchorage system tends to make fuller use of FRP sheets. It can fully develop the tensile strength of EB FRP sheets by using a much shorter bond length over the embedded spike (l_{end}=38 mm). The anchorage system even can fracture EB FRP sheets with a sharp corner (R_b=0 mm), suggesting a limited impact of bend radius on the two-patch anchorage system and a possible saving on the hole preparation.
2. FRP-concrete bond has notably impacts on the anchorage system. It suggests that a long-term bond loss due to harsh environment could compromise the capacity of the anchored FRP sheet.
3. The bond condition between the anchorage system and FRP sheet can be improved by narrowing down the fanning angle. Reducing the fanning angle from 49° to 37° successfully prevented the

unfavorable failure of anchor-sheet delamination and anchor rupture.

Acknowledgments

The support of the National Natural Science Foundation of China [grant numbers 51608244 and 51608520], Natural Science Foundation of Jiangsu Province (BK20160265), China Postdoctoral Science Foundation (2016M590516), the Key Laboratory of Ministry of Education for Mechanics on Western Disaster and Environment, and the School of Civil Engineering and Mechanics at Lanzhou University are greatly appreciated.

References

[1] Lou T, Karavasilis TL. Time-dependent assessment and deflection prediction of prestressed concrete beams with unbonded CFRP tendons. Compos Struct 2018;194:365–76. doi:10.1016/j.compstruct.2018.04.013.

[2] Lou T, Min D, Sun W, Chen B. Numerical assessment of continuous prestressed NSC and HSC members with external CFRP tendons. Compos Struct 2020;234:111671. doi:10.1016/j.compstruct.2019.111671.

[3] Lou T, Peng C, Karavasilis TL, Min D, Sun W. Moment redistribution versus neutral axis depth in continuous PSC beams with external CFRP tendons. Eng Struct 2019;209:109927. doi:10.1016/j.engstruct.2019.109927.

[4] Jiang SF, Ma SL, Wu ZQ. Experimental study and theoretical analysis on slender concrete-filled CFRP-PVC tubular columns. Constr Build Mater 2014. doi:10.1016/j.conbuildmat.2013.11.089.

[5] Sun W, Jirsa JO, Ghannoum WM. Behavior of anchored carbon fiber-reinforced polymer strips used for strengthening concrete structures. ACI Mater J 2016. doi:10.14359/51688637.

[6] Wu Y, Huang Y. Hybrid Bonding of FRP to Reinforced Concrete Structures. J Compos Constr 2008;12:266–73. doi:10.1061/(ASCE)1090-0268(2008)12:3(266).

[7] Dat Duthinh and Monica Starnes. Strengthening of Reinforced Concrete Beams with Carbon FRP. Compos Constr 2001;1:493–8.

[8] Kalfat R, Al-Mahaidi R. A prediction model for bidirectional fiber patch anchors used to enhance the performance of FRP materials bonded to concrete. Compos Struct 2014;117:51–8. doi:10.1016/j.compstruct.2014.05.034.

[9] Pham HB, Al-Mahaidi R. Prediction Models for Debonding Failure Loads of Carbon Fiber Reinforced Polymer Retrofitted Reinforced Concrete Beams. J Compos Constr 2006;10:48–59. doi:10.1061/(ASCE)1090-0268(2006)10:1(48).

[10] Al-Amery R, Al-Mahaidi R. Coupled flexural-shear retrofitting of RC beams using CFRP straps. Compos Struct 2006;75:457–64. doi:10.1016/j.compstruct.2006.04.037.

[11] Smith ST, Teng JG. Shear-Bending Interaction in Debonding Failures of FRP-Plated RC Beams. Adv Struct Eng 2003;6:183–99. doi:10.1260/136943303322419214.

[12] Niemitz CW, James R, Breña SF. Experimental Behavior of Carbon Fiber-Reinforced Polymer (CFRP) Sheets Attached to Concrete Surfaces Using CFRP Anchors. J Compos Constr 2010;14:185–94. doi:10.1061/(ASCE)CC.1943-5614.0000064.

[13] Orton SL, Jirsa JO, Bayrak O. Design Considerations of Carbon Fiber Anchors. J Compos Constr 2008;12:608–16.

[14] Villanueva Llauradó P, Ibell T, Fernández Gómez J, González Ramos FJ. Pull-out and shear-strength models for FRP spike anchors. Compos Part B Eng 2017. doi:10.1016/j.compositesb.2017.02.029.

[15] Kim. Use of CFRP to provide continuity in existing reinforced concrete members subjected to extreme loads. 2008.

[16] Sun W. Development of a testing methodology for the design and quality control of carbon fiber reinforced polymer (CFRP) anchors. Constr Build Mater 2018;164:150–63. doi:10.1016/j.conbuildmat.2017.12.192.

[17] Ozbakkaloglu T, Saatcioglu M. Tensile Behavior of FRP Anchors in Concrete. J Compos Constr 2009;13:82–92. doi:10.1061/(asce)1090-0268(2009)13:2(82).

[18] Kim SJ, Smith ST. Pullout Strength Models for FRP Anchors in Uncracked Concrete. J Compos Constr 2010;14:406–14. doi:10.1061/(asce)cc.1943-5614.0000097.
[19] Zhang HW, Smith ST. Influence of FRP anchor fan configuration and dowel angle on anchoring FRP plates. Compos Part B Eng 2012. doi:10.1016/j.compositesb.2011.11.072.
[20] Sun W, Ghannoum WM. Modeling of anchored CFRP strips bonded to concrete. Constr Build Mater 2015;85:144–56. doi:10.1016/j.conbuildmat.2015.03.096.
[21] Sun W, Liu H, Wang Y, He T. Impacts of configurations on the strength of FRP anchors. Compos Struct 2018;194:126–35. doi:10.1016/j.compstruct.2018.04.020.
[22] Zhai Z, Feng L, Li G, Liu Z, Chang X. The anti-ultraviolet light (UV) aging property of aluminium particles / epoxy composite. Prog Org Coatings 2016;101:305–8.
[23] Sun W, Liu H, He T. Development of a novel FRP composite with high-strength, largedeformation and tensile-behavior designable properties: Design concept and experimental program. Compos Part B Eng 2019;167:448–60. doi:10.1016/j.compositesb.2019.03.016.
[24] Japan Society of Civil Engineers (JSCE). Recommendation for design and con- struction of concrete structures using continuous fiber reinforcing materials. Concrete engineering series 23. Tokyo 1997; 1997.
[25] ACI committee 440. Guide for the design and construction of externally bonded FRP systems for strengthening existing structures. 1996.
[26] Lee C, Ko M, Lee Y. Bend strength of complete closed-type carbon fiber-reinforced polymer stirrups with rectangular section. J Compos Constr 2014. doi:10.1061/(ASCE)CC.1943-5614.0000428.
[27] Shehata E, Morphy R, Rizkalla S. Fibre reinforced polymer shear reinforcement for concrete members: Behaviour and design guidelines. Can J Civ Eng 2000. doi:10.1139/l00-004.
[28] Fyfe Co.LLC. Tyfo ® SCH-11UP Composite, 2015.
[29] Wight JK, McCormac J. Reinforced Concrete: Mechanics and Design. Pearson; 2015. doi:10.1680/mobe.34525.0615.
[30] Sun W, Peng X, Liu H, Qi H. Numerical studies on the entire debonding propagation process of FRP strips externally bonded to the concrete substrate. Constr Build Mater 2017;149:218–35. doi:10.1016/j.conbuildmat.2017.05.117.
[31] Sun W, Peng X, Yu Y. Development of a simplified bond model used for simulating FRP strips bonded to concrete. Compos Struct 2017;171:462–72. doi:10.1016/j.compstruct.2017.03.066.
[32] del Rey Castillo E, Griffith M, Ingham J. Straight FRP anchors exhibiting fiber rupture failure mode. Compos Struct 2019;207:612–24. doi:10.1016/j.compstruct.2018.09.073.
[33] del Rey Castillo E, Dizhur D, Griffith M, Ingham J. Experimental testing and design model for bent FRP anchors exhibiting fiber rupture failure mode. Compos Struct 2019;210:618–27. doi:10.1016/j.compstruct.2018.11.091.

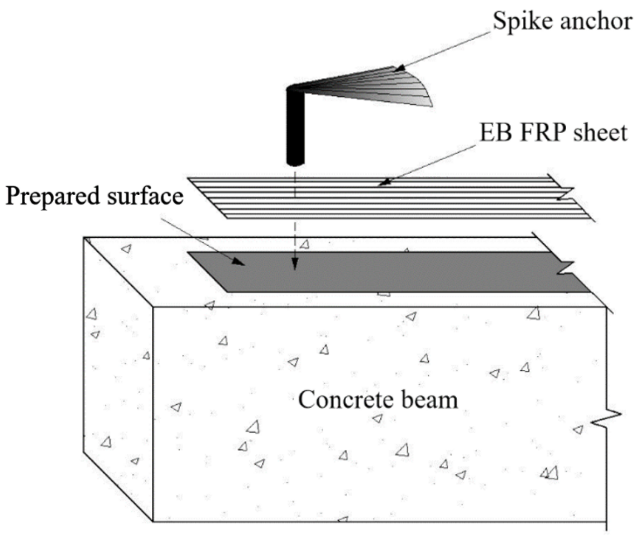

(a) Installing a typical FRP spike anchor

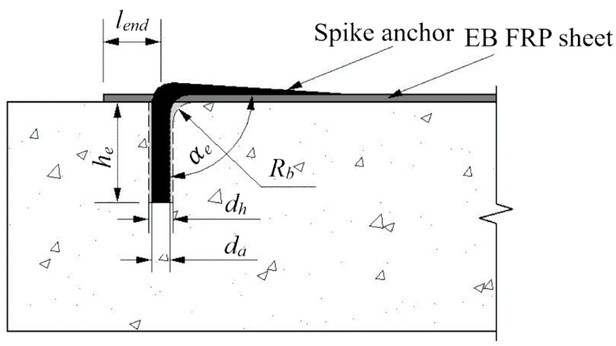

(b) Anchor details

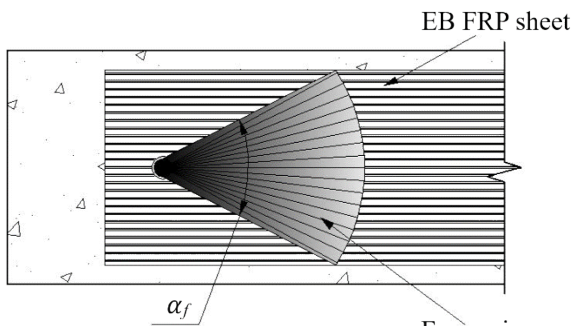

(c) A FRP spike anchor bonded onto FRP sheet

Fig.1. A typical FRP spike anchor

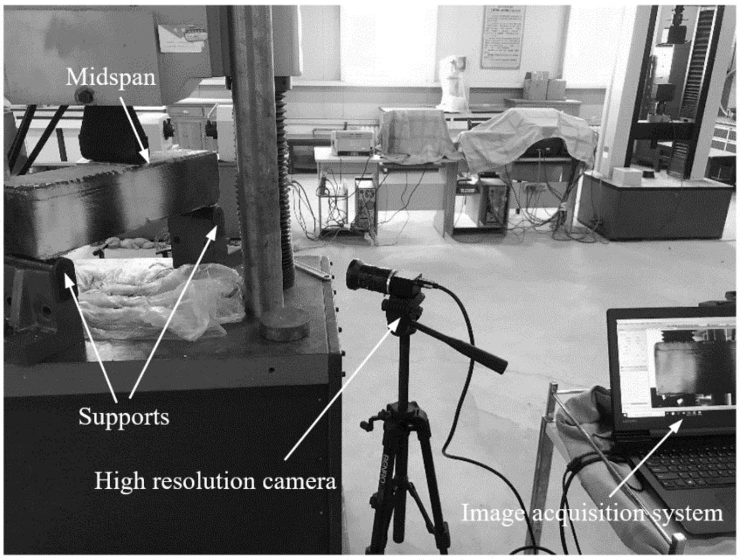

Fig.2. Three-point flexural test setup

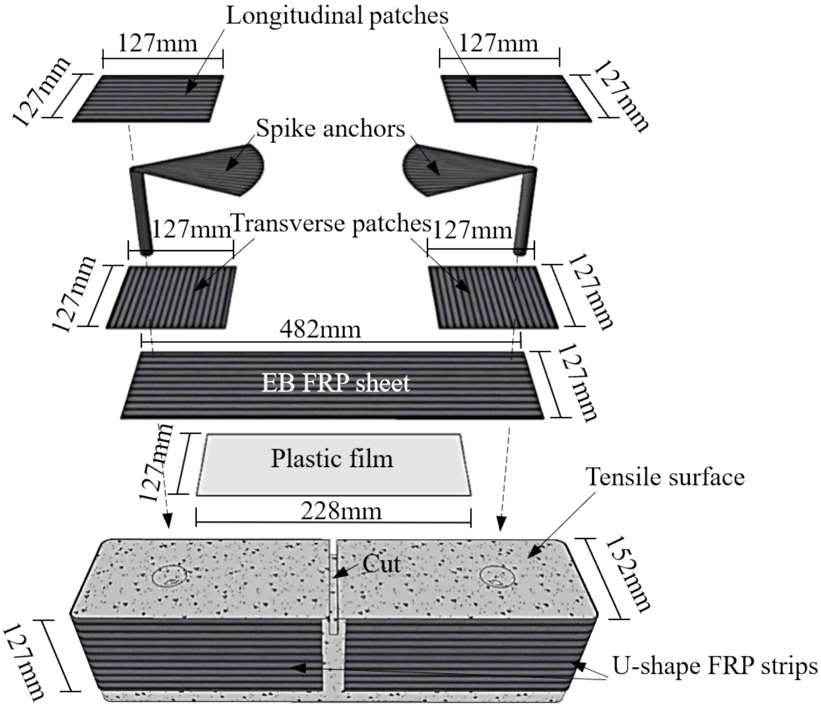

(a) FRP details

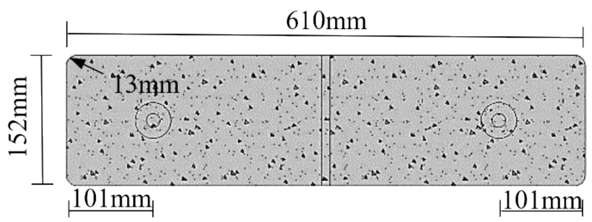

(b) Tensile surface of concrete specimen

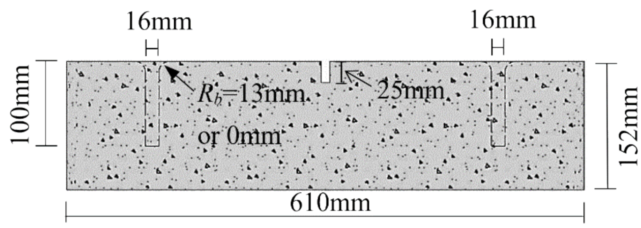

(c) Side view of concrete specimen

Fig.3. Test specimens

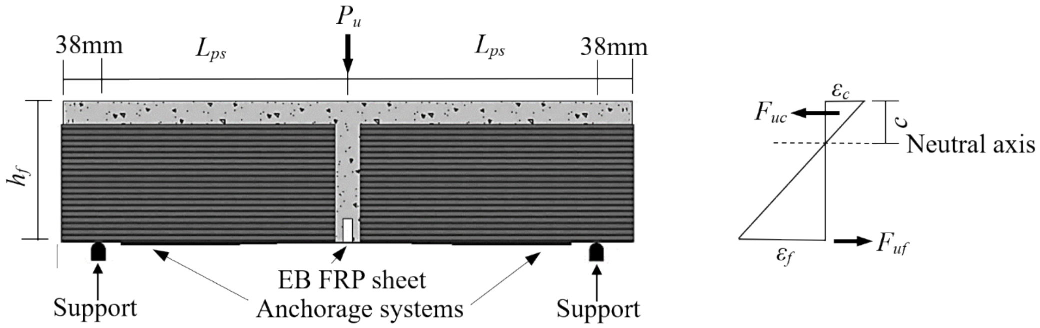

Fig.4. Beam equilibrium

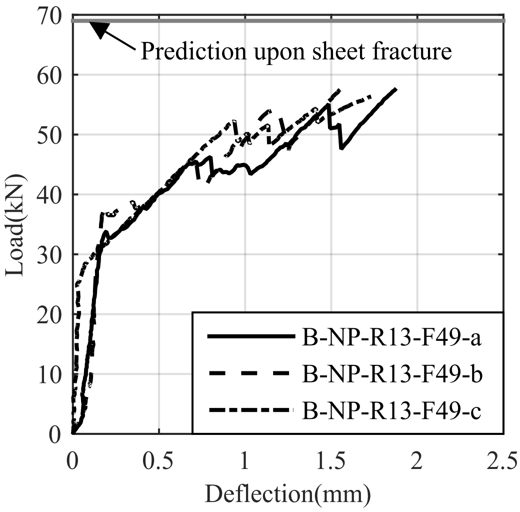

(a) Load-deflection curves

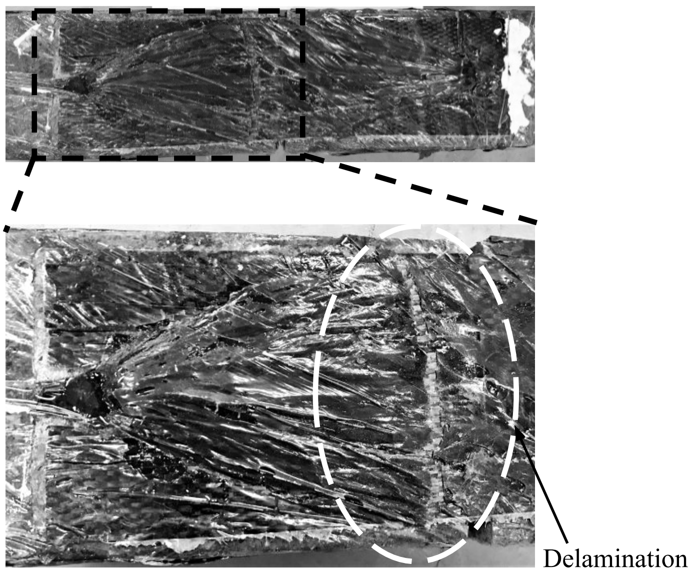

(b) Failure modes

Fig.5. Experimental results of specimens with no patches

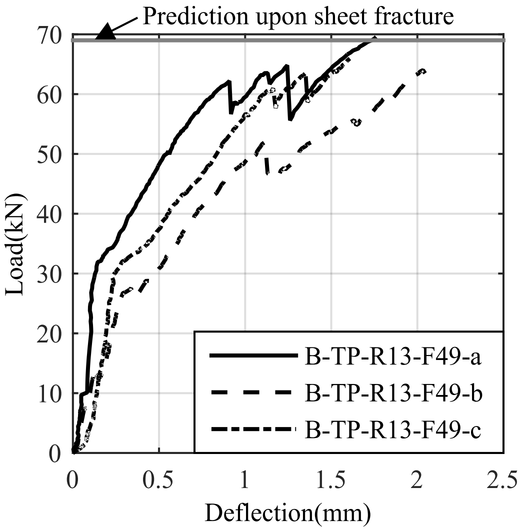

(a) Load-deflection curves

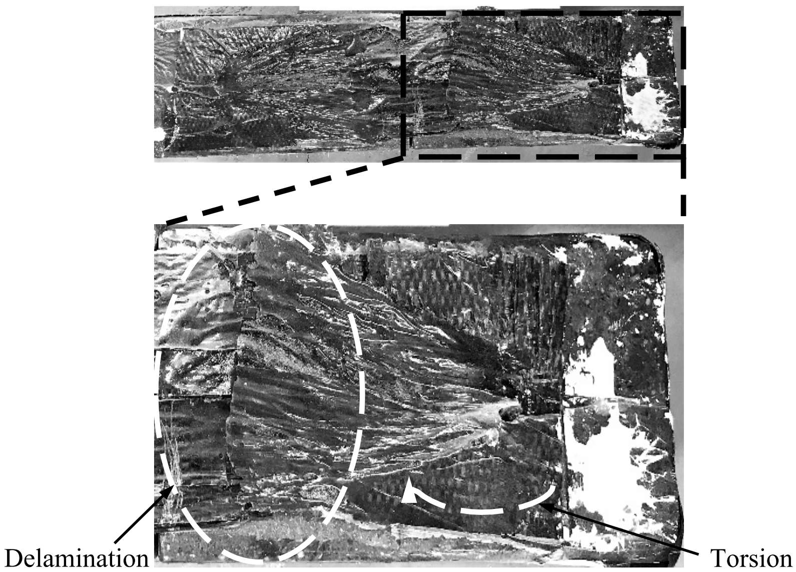

(b) Failure modes

Fig.6. Experimental results of specimens with transverse patches

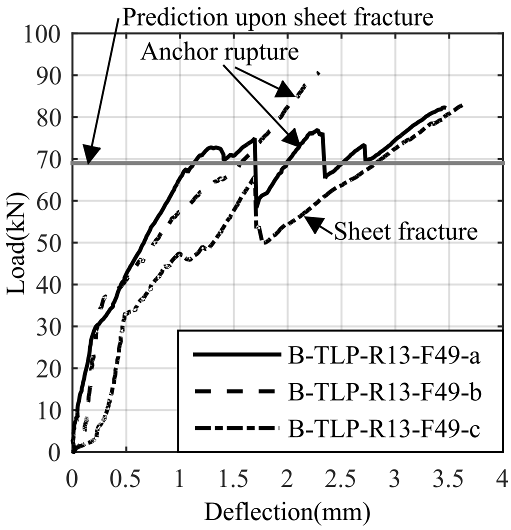

(a) Load-deflection curves

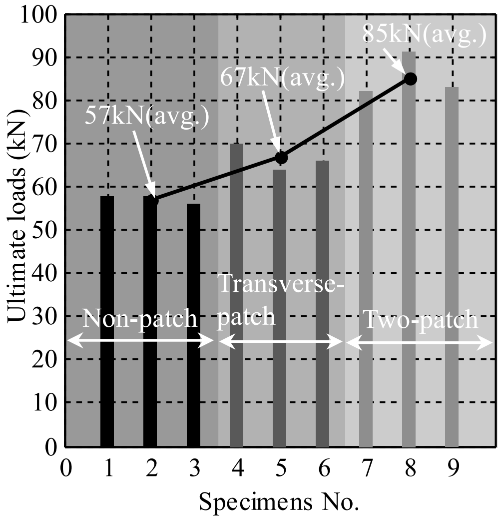

(b) Comparions of non-patch, transverse-patch, and two-patch applications

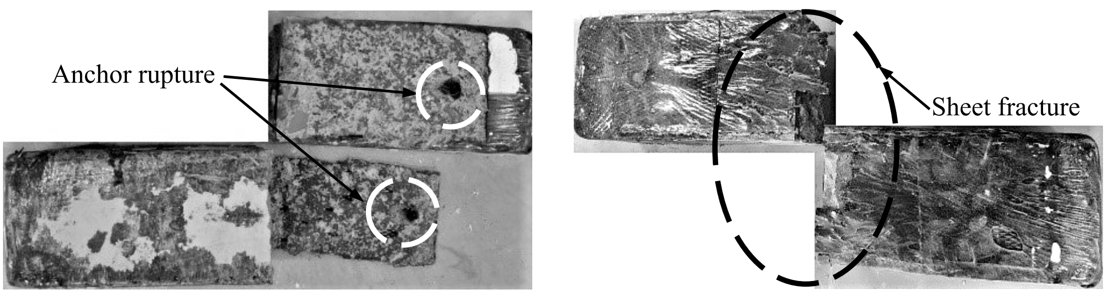

(c) Failure modes

Fig.7. Experimental results of specimens with two patches

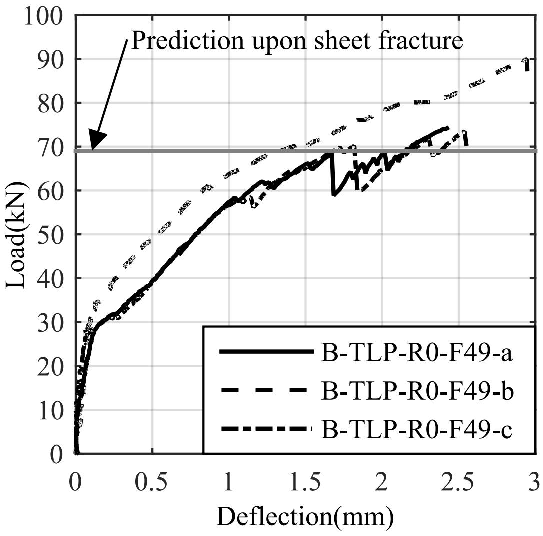

(a) Load-deflection curves

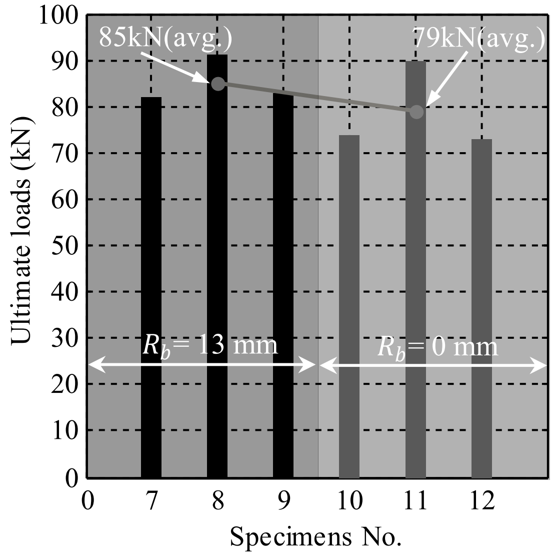

(b) Comparisons between R_b= 13 mm and R_b= 0 mm

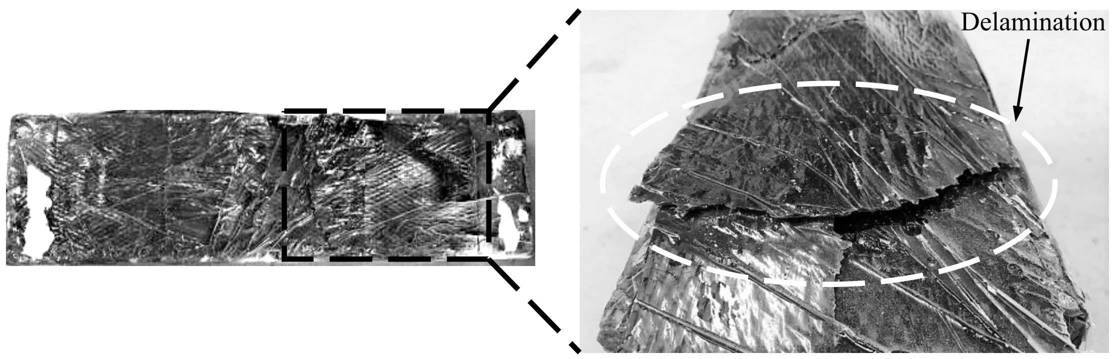

(c) Failure modes

Fig.8. Experimental results of two-patch specimens with a bend radius of 0mm

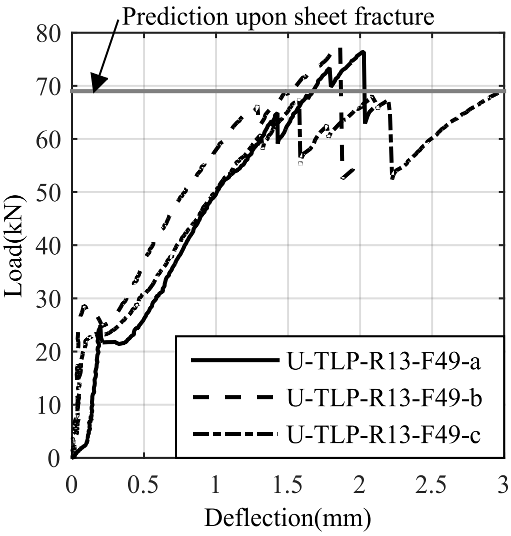

(a) Load-deflection curves

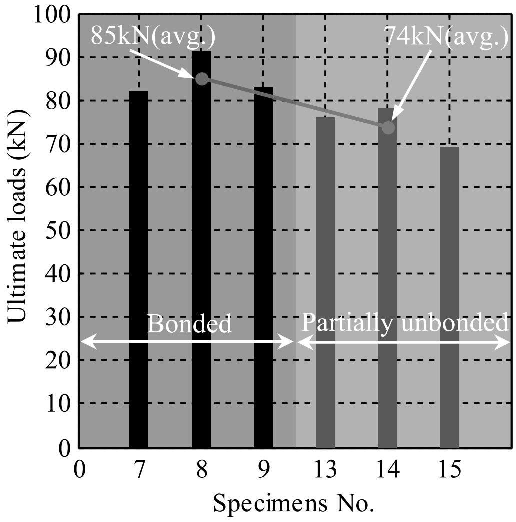

(b) Comparison between bonded and partially unbonded applications

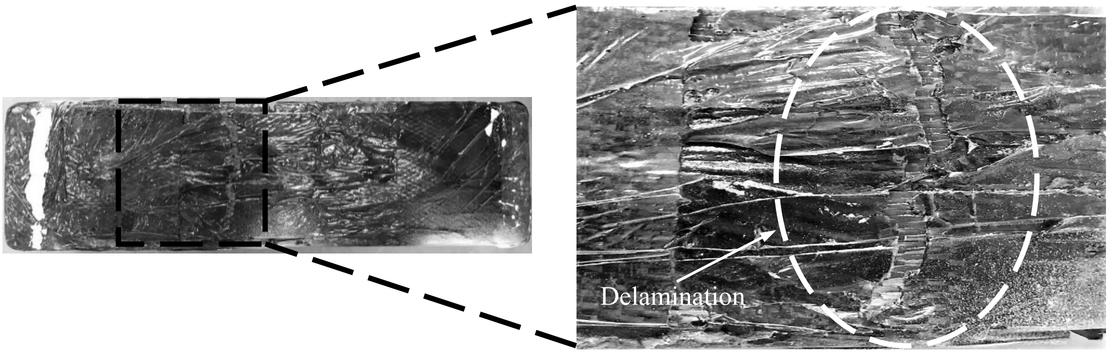

(c) Failure modes

Fig.9. Experimental results of partially unbonded specimens with two patches

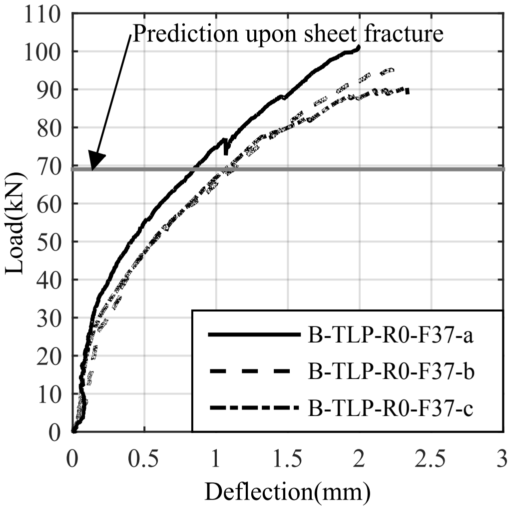

(a) Load-deflection curves

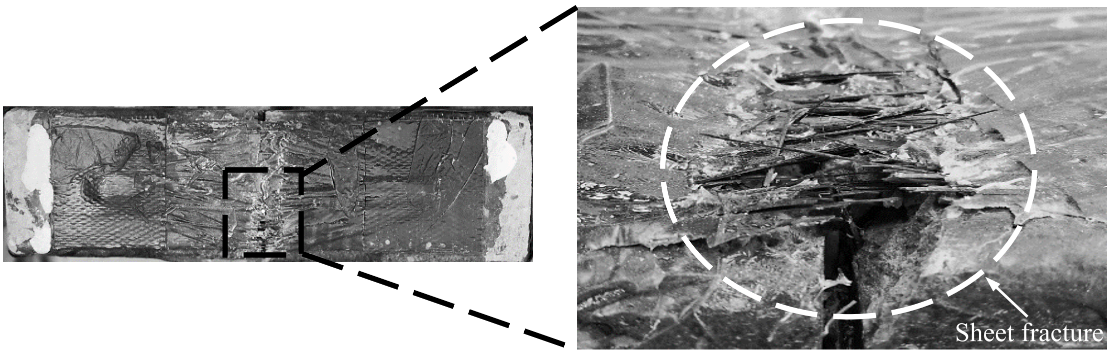

(b) Failure modes

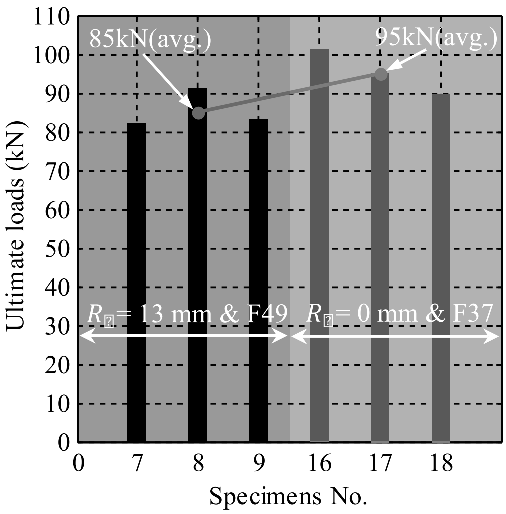

(c) Comparison between R_b= 13 mm & F49 and R_b= 0 mm & F37

Fig.10. Experimental results of specimens with a bend radius of 0 mm and fanning angle of 37°

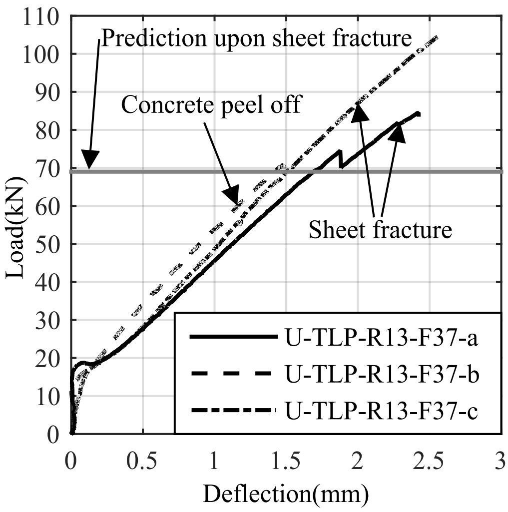

(a) Load-deflection curves

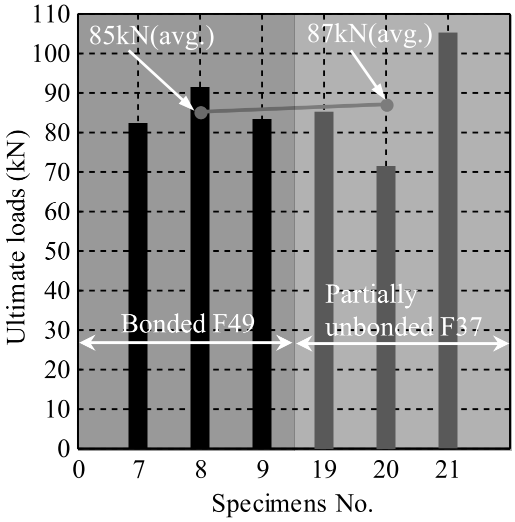

(b) Comparisons between bonded F49 and partially unbonded F37 applications

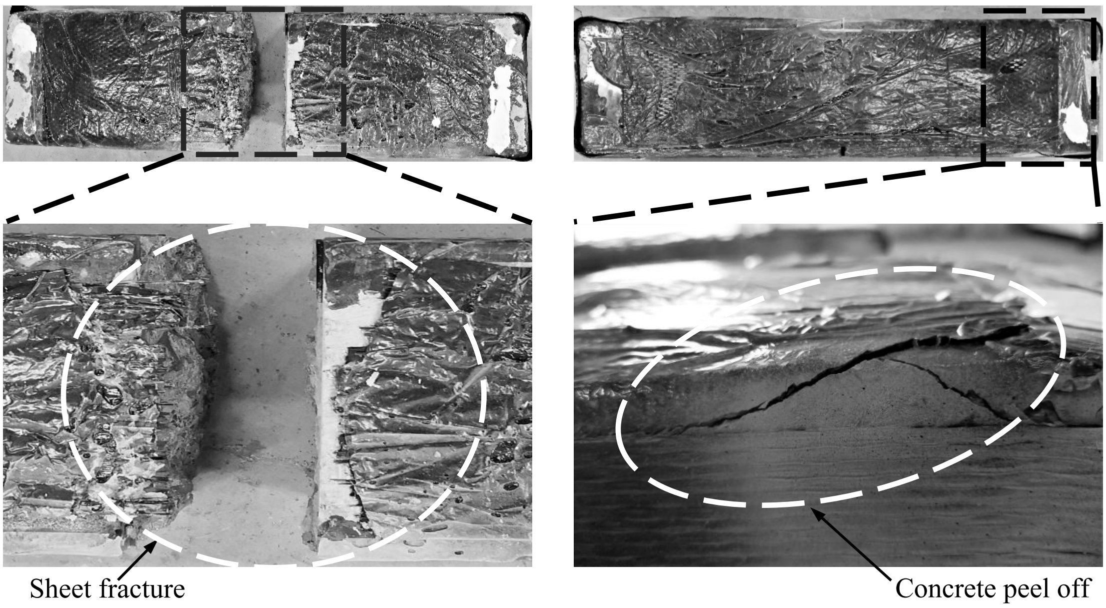

(c) Failure modes

Fig.11. Experimental results of partically unbonded specimens with fanning angle of 37°

Table 1. Specimen details

No.	Specimen ID	Bond condition	Patch details		Bend radius (mm)	Fan details		
			Transverse Patches (mm^2)	Longitudinal Patches (mm^2)		Angle (°)	Length (mm)	Area (mm^2)
1-3	B-NP-R13-F49	Bonded	----	----	13	49	153	10021
4-6	B-TP-R13-F49	Bonded	127×127	-----	13	49	153	10021
7-9	B-TLP-R13-F49	Bonded	127×127	127×127	13	49	153	10021
10-12	B-TLP-R0-F49	Bonded	127×127	127×127	0	49	153	10021
13-15	U-TLP-R13-F49	Partially Unbonded	127×127	127×127	13	49	153	10021
16-18	B-TLP-R0-F37	Bonded	127×127	127×127	0	37	200	12931
19-21	U-TLP-R13-F37	Partially Unbonded	127×127	127×127	13	37	200	12931

Table 2. Experimental results

No.	Specimens	Ultimate loads (kN)	Averages of ultimate loads (kN)	Eq.(1) resulted in f_{fb}/ P_u (MPa/ kN)	Eq.(2) resulted in f_{fb}/ P_u (MPa/ kN)	Eq.(4) resulted in f_{fb}/ P_u (MPa/ kN)	Eq.(5) resulted in f_{fb}/ P_u (MPa/ kN)	Measured P_u resulted in f_{fb} (MPa)	Failure modes
1	B-NP-R13-F49-a	58		514/72	346/49	247/35	365/51	413	Delamination
2	B-NP-R13-F49-b	58	57	514/72	346/49	247/35	365/51	413	Delamination
3	B-NP-R13-F49-c	56		514/72	346/49	247/35	365/51	399	Delamination
4	B-TP-R13-F49-a	70		514/72	346/49	247/35	365/51	500	Delamination
5	B-TP-R13-F49-b	64	67	514/72	346/49	247/35	365/51	457	Delamination
6	B-TP-R13-F49-c	66		514/72	346/49	247/35	365/51	471	Delamination
7	B-TLP-R13-F49-a	82		514/72	346/49	247/35	365/51	588	Anchor rupture
8	B-TLP-R13-F49-b	91	85	514/72	346/49	247/35	365/51	654	Anchor rupture
9	B-TLP-R13-F49-c	83		514/72	346/49	247/35	365/51	595	Sheets fracture
10	B-TLP-R0-F49-a	74		444/62	296/42	197/28	305/43	529	Delamination
11	B-TLP-R0-F49-b	90	79	444/62	296/42	197/28	305/43	647	Delamination
12	B-TLP-R0-F49-c	73		444/62	296/42	197/28	305/43	522	Delamination
13	U-TLP-R13-F49-a	76		514/72	346/49	247/35	365/51	544	Delamination
14	U-TLP-R13-F49-b	78	74	514/72	346/49	247/35	365/51	558	Delamination
15	U-TLP-R13-F49-c	69		514/72	346/49	247/35	365/51	493	Delamination
16	B-TLP-R0-F37-a	101		444/62	296/42	197/28	305/43	729	Sheets fracture
17	B-TLP-R0-F37-b	95	95	444/62	296/42	197/28	305/43	684	Sheets fracture
18	B-TLP-R0-F37-c	90		444/62	296/42	197/28	305/43	647	Sheets fracture
19	U-TLP-R13-F37-a	85		514/72	346/49	247/35	365/51	610	Sheets fracture
20	U-TLP-R13-F37-b	71	87	514/72	346/49	247/35	365/51	507	Concrete peel off
21	U-TLP-R13-F37-c	105		514/72	346/49	247/35	365/51	760	Sheets fracture